



pubs.acs.org/JPCB Article

Interfacial Inversion, Interference, and IR Absorption in Vibrational Sum Frequency Scattering Experiments

S. Pullanchery, L. Zhang, S. Kulik, and S. Roke*



Cite This: J. Phys. Chem. B 2023, 127, 6795-6803



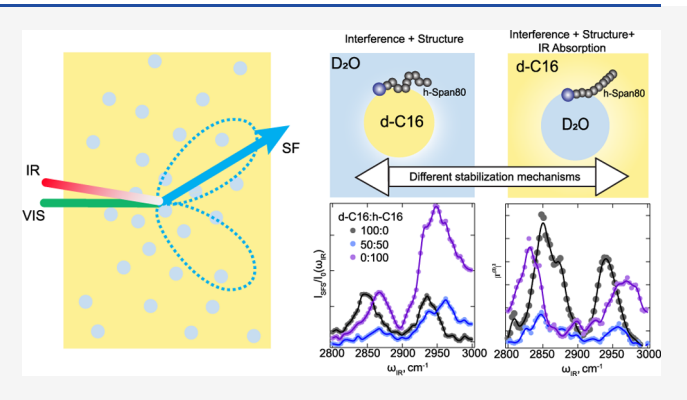
ACCESS I

Metrics & More

Article Recommendations

Supporting Information

ABSTRACT: Molecular interfacial structure greatly determines the properties of nano- and microscale systems. Vibrational sum frequency scattering (SFS) spectroscopy is a unique interface-selective tool to measure the interfacial vibrational spectrum of submicron to micron-scale objects dispersed in liquid and solid media. The interfacial structure is extracted from the interfacial susceptibility, a physical property derived from the intensity. Here, we describe the effect of infrared absorption that occurs in a bulk medium that is spectroscopically complex and use the results to investigate the effects of interfacial inversion, interfacial interference, and interfacial interference combined with absorption. We use the same three chemicals to do so, hexadecane oil, water, and a neutral Span80 surfactant. For all cases, the effective surface



susceptibility can be retrieved from the intensity. We further find that inverting the phases results in different interfacial structures, even though they are composed of the same three chemicals, and explain this in terms of the different interactions that are necessary to stabilize the drops: steric stabilization for water drops in oil vs. charge stabilization for oil drops in water. Interfacial interference can be used to estimate the surface density of different compounds.

■ INTRODUCTION

The orientation and conformation of molecules at an interface determine its physical and chemical properties. Therefore, understanding the interfacial molecular structure is essential for various processes in chemistry and biology. Vibrational sum frequency generation (SFG) spectroscopy is a highly interfaceselective technique that can elucidate the interfacial molecular structure.¹⁻⁵ Sum frequency (SF) photons can be generated when two ultrafast laser beams of infrared (IR) and visible (VIS) frequencies are spatially and temporally overlapped, requiring a simultaneous IR and Raman transition. Coherent SF photons arise from anisotropic molecules that assume a non-centrosymmetric ordering and are therefore not generated in an isotopic bulk liquid (under the electric-dipole approximation). Because interfaces are generally characterized by anisotropy along the surface normal, the SF intensity is generated only from the interface. The vibrational sum frequency spectra contain information about the surface density and orientation of molecules at the interface. SFG has been extensively used to study extended planar surfaces such as air/water, surfactant/water, lipid/water, protein/water, oil/water, and many other interfaces. 1,6-17 The average tilt angle of different molecular groups at the interface has been estimated from SF measurements under different polarization combinations. However, such earlier SFG measurements were limited to extended planar interfaces, whereas most of the

interfaces in nature have micro- or nanoscale structures/length scales.

To study the molecular structure of droplet and particle interfaces immersed in liquid media, vibrational sum frequency scattering (SFS) spectroscopy was invented. 22,23 SFS spectroscopy involves spatially and temporally overlapping ultrafast IR and VIS laser beams inside a medium that contains the particles or objects of interest while recording the scattered SF photons. The scattered SF photons from nano- or micron-sized particle interfaces are described by the particle surface susceptibly $|\Gamma^{(2)}|^2$, which is a weighted sum of $\chi^{(2)}$ elements, with the weighing coefficients being determined by the particle size, shape, and scattering geometry.²⁴ Vibrational SFS was first demonstrated from stearyl-coated silica colloids dispersed in CCl₄. ²² In this experiment, bulk chemicals were employed that were transparent in the vibrational mode region (C-H stretch modes) of the stearyl-coated surface, enabling a clean proof of concept. Subsequently, vibrational SFS was implemented to understand the interfacial molecular structure of colloids

 Received:
 April 25, 2023

 Revised:
 June 26, 2023

 Published:
 July 20, 2023





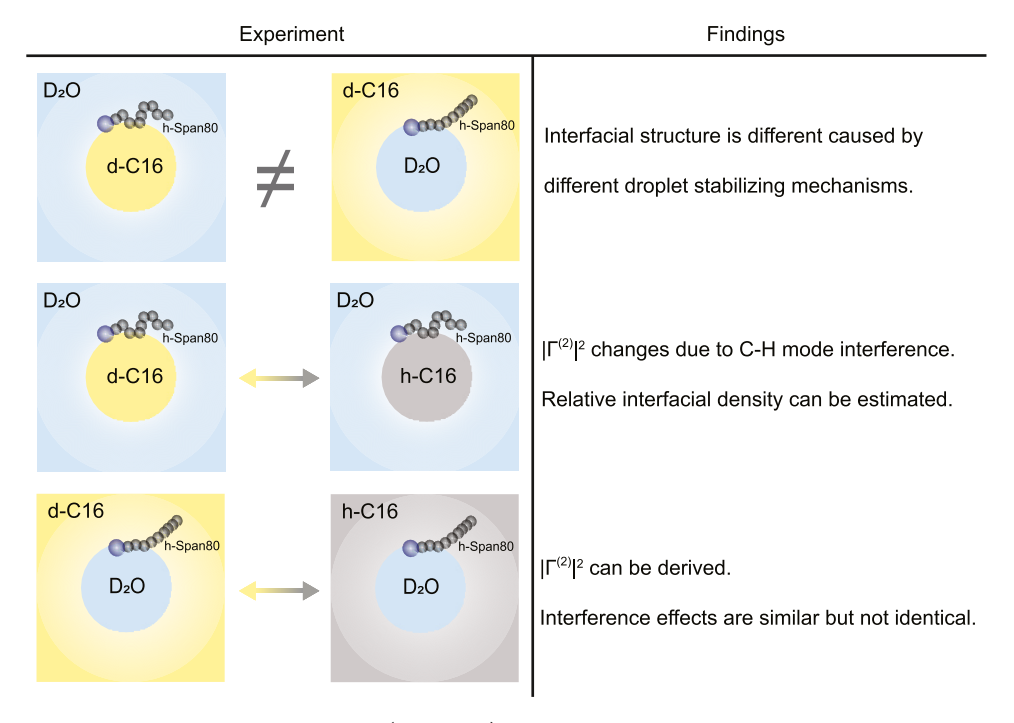


Figure 1. Graphical illustration of experiments and findings. (Top panel) Interfacial inversion: h-Span80 on the surface of oil-in-water and water-in-oil droplets. (Middle panel) Interfacial interference: h-Span80 on the surface of oil-in-water droplets. The oil phase is isotopically diluted with d-C16:h-C16 mixtures. (Bottom panel) Combined interference and absorption: h-Span80 on the surface of water-in-oil droplets. The oil phase is isotopically diluted with d-C16:h-C16 mixtures.

undergoing phase transitions, ^{25,26} structural heterogeneities in polymeric particles, ^{27,28} bare oil droplets in water, ^{29–32} surfactant-covered oil droplets, ^{33–38} lipid (nano)droplets, and liposomes. ^{39–42} Recently, more complex systems have also been studied, including protein fibers in solution, ⁴³ peptides at emulsion interfaces, ⁴⁴ and polycations at lipid membrane surfaces. ⁴⁵

The first vibrational SFS proof of concept study deliberately employed a surface layer with a unique vibrational mode so that the response in this frequency range would have to originate from the interface. However, this is not the case for most common systems, and when this is not the case, the emitted SF photons are influenced not only by the molecular structure but also by interference and linear absorption. For droplet systems, these effects can be circumvented by using selective deuteration of the dispersed (oil) phase. When the oil phase is selectively deuterated, the SFS spectrum of the C-H stretch region provides information about the structure and orientation of specific surfactants or oil molecules at the interface that have not been deuterated. For lipid nanodroplets, for example, the average area occupied by a single lipid molecule was estimated from the peak amplitude ratios of the CH₂ and CH₃ symmetric stretch modes. ³⁹ Furthermore, the amplitude ratios of the CH3 symmetric and asymmetric modes were used to estimate the average molecular tilt angle.³⁹ Such measurements were also possible because the bulk medium in which the droplets are dispersed was largely transparent for the infrared excitation pulse. However, this is not always the case: when the bulk medium becomes absorptive to the infrared beams, spectral acquisition and the retrieval of the surface susceptibility $|\Gamma^{(2)}|^2$, which contains the interfacial response, become more challenging.

The effect of IR absorption on the scattered SF intensity from objects dispersed in water was theoretically described

recently. He absorption by bulk water drastically modifies the SF intensity of interfacial water vibrational stretch modes. As a result of IR absorption, apparent peak frequency shifts and the presence of a spectral artifact were observed. Therefore, a theoretical framework to correct for the IR absorption was described and implemented to retrieve the interfacial water $|\Gamma^{(2)}|^2$ spectrum next to bare oil droplets in water. This framework can be applied to any spectral region to retrieve the true SF $|\Gamma^{(2)}|^2$ response from an absorptive medium. However, the effect of IR absorption can also be convoluted with other factors that change the SF spectral intensity. For example, the effect of interference and interfacial molecular structure on vibrational SF spectra has been described before.

Here, we further investigate the interfacial structure and how it can be retrieved using vibrational SFS. Having the possibility to also correct for IR absorption, we can now systematically investigate a number of interfacial phenomena that are unique for SFS from droplets: (1) interfacial inversion, (2) interfacial interference, and (3) combined absorption and interfacial interference. In each experiment, the system is composed of the same three chemicals: hexadecane as the oil (either deuterated hexadecane, d-C16, or hydrogenated hexadecane, h-C16), Span80 as a neutral surfactant, and water (D₂O). Figure 1 illustrates how these 3 effects are implemented and summarizes our findings. Inverting the interface results in different $|\Gamma^{(2)}|^2$ spectra and Span80 interfacial structures that reflect the different droplet-stabilizing mechanisms for water droplets in oil (water-in-oil) or oil droplets in water (oil-inwater) (Figure 1, top). Interference leads to distinctly different spectra that might be used to infer statements about the surface density (Figure 1, middle). When interference and absorption both play a role (Figure 1, bottom), it is still possible to retrieve the $|\Gamma^{(2)}|^2$ spectrum, which provides

encouraging prospects for future studies using vibrational SFS on more complicated systems.

This work is structured as follows: We start with theoretical considerations for retrieving the effective absolute square of the particle's surface susceptibility $|\Gamma^{(2)}|^2$, which represents the pure interfacial response. We examine the effect of the spectrally complex IR absorption from the main bulk phase and consider how it influences the emitted SF intensity. We also consider the effect of the spectral resolution of the instrument on the retrieval of $|\Gamma^{(2)}|^2$. This is followed by experiments in the Results and Discussion section that demonstrate interfacial inversion (Figure 3), interfacial interference (Figure 4), and interfacial interference combined with linear IR absorption (Figure 5).

MATERIALS AND METHODS

Chemicals. Hexadecane ($C_{16}H_{34}$, C16, 99.8%, Sigma-Aldrich), d_{34} -hexadecane (98% D, Cambridge Isotope), D₂O (99.8% D, Thermo Scientific), Sorbitane monooleate, Span80 (Sigma-Aldrich) were used as received. The glassware used for preparing and storing nano-emulsions was cleaned with a freshly prepared piranha ($H_2SO_4/H_2O_2=3:1$) solution. After being immersed in piranha for ~20 min, the glassware was rinsed thoroughly with ultrapure water (18.2 MΩ·cm) obtained from a Milli-Q UF-Plus instrument (Millipore Inc.).

Sample Preparation and Characterization. The nanodroplets were prepared using a two-step process. First, all the ingredients were mixed in a 4 mL glass vial and homogenized using a hand-held homogenizer (TH, OMNI International) at an angular velocity of 15 rpm for 3-5 min. Afterward, nanoemulsions were obtained by sonicating in an ultrasonic bath (35 kHz, 400 W, Bandelin) for 3-10 min. The size distribution of droplets studied had average diameters varying between ~100 and 300 nm (SI Table S2), which was characterized by dynamic light scattering (DLS) via a Malvern ZS nanosizer instrument. The stock emulsions were prepared using 2 vol % droplets. For isotope dilution measurements of water-in-oil droplets, a series of samples with 1 vol % were obtained by diluting the same stock dispersions of nanodroplets with various h-C16:d-C16 mixtures so as to keep the size distribution constant throughout the experiment.

FTIR spectra were measured using a Bruker Vertex 70 spectrometer equipped with Ag mirrors in transmission mode. A 10 μ m thick sample cell composed of CaF₂ (front) and quartz (back) windows was used to collect FTIR spectra for normalization.

Vibrational Sum Frequency Scattering. In the vibrational SFS spectroscopy system, IR and VIS pulsed laser beams are temporally and spatially overlapped inside the sample cuvette. The experimental setup has been previously described in detail in refs. ^{47–49} The broad IR pulses (3.4 μ m, 10 μ J, with a full width at half-maximum (FWHM) of 180 cm⁻¹) were obtained from an OPA system (HE-TOPAS-C, Light Conversion) with a Ti:sapphire femtosecond pump laser system (800 nm, 1 kHz, Spitfire Pro, Spectra physics). The output from the pump laser was split, with the first part being used to generate IR photons, as described, and the second part being directed into a home-built pulse shaper that generated the narrow VIS pulses (800 nm, 10 μ J, FWHM = 15 cm⁻¹). The polarization of the IR beam was controlled by BaF2 two wire-grid polarizers. The polarization of the VIS beam was controlled by a polarizer cube (CVI, PBS-800-050) and a halfwave plate (EKSMA, 460–4215). The IR and VIS beams were

focused under an opening angle of 15° into a cuvette having CaF₂ (front) and quartz (back) windows. The cuvette has an optical path length of 200 μ m. The emitted SF light was collected and collimated using a plano-convex lens (f = 15mm, Thorlabs LA1540-B) at the scattering angle that aligned with the broad maximum intensity of the scattering patterns, which is at $\theta = 57^{\circ}$ as measured in air. The SFS light was spectrally filtered by two short-pass filters (3rd, Millenium, 3RD770SP), and its polarization was controlled with a Glan-Taylor prism (Thorlabs, GT15-B), after which it was spectrally dispersed with a monochromator (Acton, SpectraPro 2300i) and then detected by a gated intensified CCD camera (Princeton Instrument, PI-Max3) with a gate width of 10 ns. The acquisition time for a single C-H spectrum was 600 s. Prior to absorption correction, the measured sum frequency spectra were normalized by the incident IR spectrum $(I_0(\omega_{IR}),$ recorded from barium titanate nanoparticles), VIS and IR pulse energies, and acquisition time. The intensities were further size-normalized using the average value of the droplet radii⁴⁷ by dividing by R³, where R is the droplet radius (DLSderived values of the average droplet diameter and PDI are given in Table S2). The SFS spectra that are reported in this work were recorded using P-polarized (parallel to the horizontal scattering plane) IR and S-polarized (perpendicular to the horizontal scattering plane) SF and VIS beams, respectively, abbreviated as the SSP polarization combination. The C-H stretching spectra were fitted using Levenberg-Marquadt iterations using the equation

$$I_{\text{SFS}}(\omega_{\text{IR}}, \theta) \propto \left| A_{\text{NR}} f(\omega_{\text{IR}}) e^{i\phi_{\text{NR}}} + \sum_{v} \frac{A_{v}(\theta) \gamma_{v}}{\omega_{\text{IR}} - \omega_{v} + i\gamma_{v}} \right|^{2}$$

$$(1)$$

where $A_{\rm NR}$, $f(\omega_{\rm IR})$, and $\varphi_{\rm NR}$ are the amplitude, shape, and phase of non-resonant background, $A_{\rm v}(\theta)$, $\omega_{\rm v}$, and $\gamma_{\rm v}$ denote the amplitude, frequency, and linewidth of resonant vibrational modes.

Theoretical Background and Considerations. Theoretical description of vibrational SFS in adsorptive media. As has been described earlier, ²³ for the measurements in a non-absorptive medium, the intensity of SFS light is proportional to the intensities of the IR and VIS beams

$$I(\omega_{\rm SF} = \omega_{\rm IR} + \omega_{\rm vis}) \propto |\Gamma^{(2)}|^2 I_{\rm IR}(\omega_{\rm IR}) I_{\rm vis}(\omega_{\rm vis})$$
 (2)

where $I_{\rm IR}(\omega_{\rm IR})$ and $I_{\rm vis}(\omega_{\rm vis})$ are the incident intensities of IR and VIS beams, respectively, and $\Gamma^{(2)}$ is the effective second-order particle susceptibility. $\Gamma^{(2)}$ is determined by the second-order surface susceptibility ($\chi^{(2)}$), the scattering angle (θ , the angle between the scattered SF wavevector and that of the sum of the IR and VIS wavevectors), and the radius of the particle. After incident intensity normalization by the IR and VIS beams, the $|\Gamma^{(2)}|^2$ spectrum containing spectral information about the interfacial responses is obtained. However, this intensity normalization is not sufficient to extract the $|\Gamma^{(2)}|^2$ responses of particle interfaces in an absorptive medium. As light propagates through an absorptive medium along direction z, the IR beam's frequency resolved intensity profile attenuates and changes dramatically along z. The intensity at distance z is described by

$$I_{\rm IR}(\omega_{\rm IR}, z) = I_0(\omega_{\rm IR}) e^{-\alpha(\omega_{\rm IR})z}$$
(3)

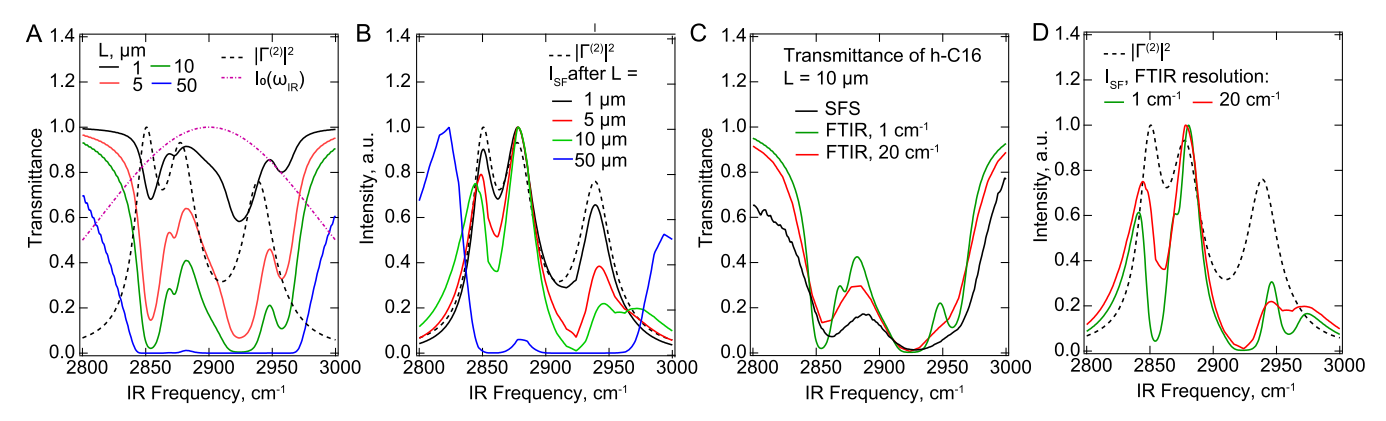


Figure 2. Simulation of the effects of absorption in the C–H stretch mode region. (A) IR transmission spectra of n-hexadecane for different optical path lengths (L) and inputs used for $|\Gamma^{(2)}|^2$ and $I_0(\omega_{\rm IR})$. (B) Computed $I(\omega_{\rm SF}=\omega_{\rm IR}+\omega_{\rm vis})$ using eq 4 for the different optical path lengths using the IR transmission spectra of panel A. (C) IR transmission spectra recorded at different frequency resolutions (1 and 20 cm⁻¹), and IR transmittance spectrum from the SFS setup. (D) Computed SFS intensity spectra using eq 4 and the $|\Gamma^{(2)}|^2$ and $I_0(\omega_{\rm IR})$ inputs of panel A, using 1 and 20 cm⁻¹ resolution FTIR spectra for correction.

where $I_0(\omega_{\rm IR})$ is the incident intensity and $\alpha(\omega_{\rm IR})$ is the absorption spectrum. According to the Beer–Lambert law, the $\alpha(\omega_{\rm IR})$ is calculated from the IR transmission spectrum by $\alpha(\omega_{\rm IR}) = -\frac{\ln(T(\omega_{\rm IR}))}{L}$, where L is the optical path length. The SF intensity generated over a distance L can be expressed as

$$\begin{split} I(\omega_{\rm SF} &= \omega_{\rm IR} + \omega_{\rm vis}) \\ &\propto \int_0^L |\Gamma^{(2)}|^2 I_{\rm IR}(\omega_{\rm IR},\,z) I_{\rm vis}(\omega_{\rm vis},\,z) f_{\rm focal}(z) \rho(z) {\rm d}z \end{split} \tag{4}$$

where $I_{\rm vis}(\omega_{\rm vis},z)$ is the intensity of the visible beam at distance z, which is reduced due to linear scattering, given by, $I_{\rm vis}(\omega_{\rm vis},z)=I_0(\omega_{\rm vis})e^{-\tau_{\rm vis}z}$. Here, $I_0(\omega_{\rm vis})$ is the incident visible intensity and $\tau_{\rm vis}$ is the turbidity. Assuming the difference in refractive index between the droplets and medium is negligible, which is often the case for liquids with sub-micron-sized droplets (Rayleigh–Gans–Debye approximation), we can neglect this linear scattering effect of the VIS beam. $f_{\rm focal}(z)$ is the collection function, which quantifies the ability to collect SF response from different depths in the sample, and $\rho(z)$ is the particle/droplet number density. For SF measurements in absorptive media, the measured SF intensity can be used to retrieve $|\Gamma^{(2)}|^2$ via 30,46

$$|\Gamma^{(2)}|^2 \propto \frac{I(\omega_{\rm SF} = \omega_{\rm IR} + \omega_{\rm vis})}{\int_0^L I_{\rm IR}(\omega_{\rm IR}, z) I_{\rm vis}(\omega_{\rm vis}, z) f_{\rm focal}(z) \rho(z) dz}$$
(5)

Simulation of the IR absorption effect when oil is the main phase. Previously, we have demonstrated that the above-described procedure works well when the IR beam probes O-D stretch modes in D_2O^{30} or mixtures of H_2O and D_2O^{31} To determine the same processes when oil is the main phase, we need to further consider that the vibrational spectrum of oil (hexadecane in this case) is much more structured than that of water. This is illustrated in Figure 2A, where IR transmission spectra of hexadecane are shown for different optical path lengths. Before considering the retrieval of $|\Gamma^{(2)}|^2$ from the measured intensity, we first take the opposite approach: we use a hypothetical $|\Gamma^{(2)}|^2$ spectrum and IR intensity input profile $(I_0(\omega_{\rm IR}), \ plotted \ in Figure 2A, \ dotted \ dashed \ line)$ and compute the expected intensity $I(\omega_{\rm SF}, L)$ for different optical path lengths (Figure 2B), using eq 4. To do so, the function

under the integral in eq 4 was numerically computed for small distances $dz = 1 \mu m$ and summed over until L. For the spectral input, $|\Gamma^{(2)}|^2$, we used Lorentzian curves resembling typical peaks in the C–H stretch region (Figure 2A, black dashed line; The parameters used for simulating the Lorentzian curves are given in Table S1).

To model the incident IR profile, $I_0(\omega_{\rm IR})$, we used a Gaussian centered at 2900 cm⁻¹ with a FWHM of 200 cm⁻¹ (Figure 2A, purple dotted dashed line). The bulk medium was chosen to be pure hexadecane. Figure 2B shows the simulated SF intensity for the given inputs (eq 4). The relative intensities of the C–H modes vary significantly due to IR absorption. With increasing optical probing thickness (L) from 1 μ m (Figure 2B black) to 10 μ m (Figure 2B green), the spectral shape changes significantly: The apparent d⁺/r⁺ ratio decreases, the apparent center frequency of the d⁺ mode shifts to lower frequencies, and the relative intensity above 2950 cm⁻¹ increases. Without absorption correction, these spectra would have been drastically misinterpreted to originate from different surface structures.

Besides having multiple peaks, there is another element that enters the analysis and that is the frequency resolution of the SFS instrument. The IR absorption/transmittance spectra that are used for correction need to be recorded with a frequency resolution that matches that of the SFS instrument. Figure 2C shows the elements necessary for considering this effect: IR transmission spectra recorded from 10 µm path length hexadecane with 1 and 20 cm⁻¹ resolution using an FTIR spectrometer, together with an IR transmission spectrum recorded from the SFS setup. To measure the IR transmittance spectrum from the SFS setup, a 10 μ m thick sample containing hexadecane was placed in the IR beam path of the SFS instrument while recording the IR profile. The IR profile measured with an empty cuvette in the IR path was used as the reference. The transmitted IR spectrum was obtained by dividing the obtained IR spectra from the sample by that from the reference. Using the IR absorption spectra with different resolutions together with the same $|\Gamma^{(2)}|^2$ in eq 4 results in different intensity spectra, as plotted in Figure 2D. Therefore, to obtain the actual $|\mathbf{\Gamma}^{(2)}|^2$ spectrum, it is important to perform the absorption correction using IR spectra that have been recorded with the same resolution as that of the SFS spectrometer.

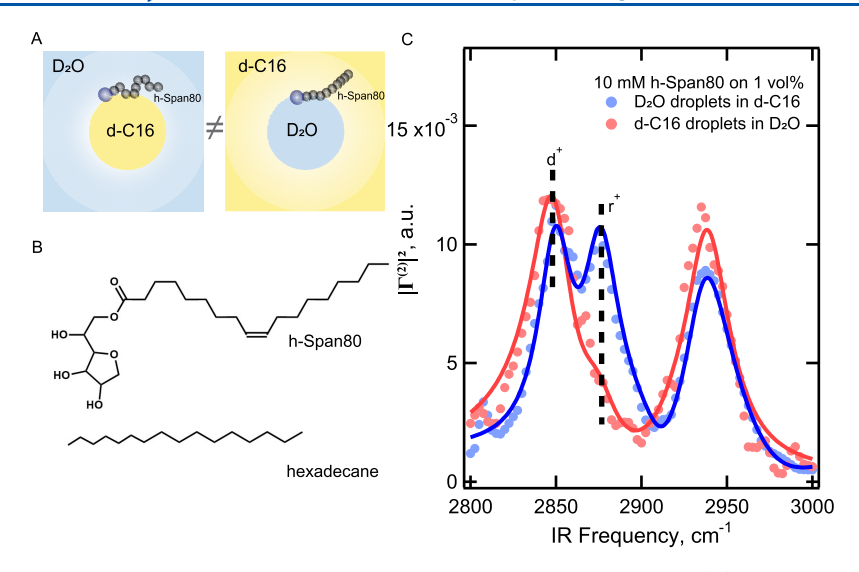


Figure 3. The structure of Span80 on hexadecane—water interfaces, formed as inverse droplet systems. (A) Schematic illustration of two chemically identical interfaces present in the two different types of droplet systems studied here. (B) Chemical structure of Span80 and hexadecane. (C) SFS C—H stretch spectra of 10 mM Span80 at interfaces of oil-in-water droplets (red markers) and water-in-oil droplets (blue markers) measured under SSP polarization combination. Solid lines represent spectral fits obtained using eq 1 in Methods. The spectra were normalized to the area to enable a comparison of relative peak amplitudes.

In the next section, we will use these considerations to retrieve the $|\Gamma^{(2)}|^2$ spectra recorded from the different samples sketched in Figure 1 to investigate the effects of droplet interface inversion, interfacial interference, as well as structure, interference, and absorption on the appearance of vibrational SFS spectra.

RESULTS AND DISCUSSION

We next investigate the three aspects that can modify vibrational SFS spectra from nano-objects: interfacial inversion, interfacial interference, and absorption and interference, as summarized in Figure 1.

Interfacial Inversion. Nanodroplets of d-C16 in D_2O and D_2O in d-C16, so both stabilized by the neutral surfactant Span80 (Figure 3A,B), were prepared using ultrasonication (Materials and Methods, and Table S2 for the droplet radii). Figure 3C shows the $|\Gamma^{(2)}|^2$ spectra of the C–H stretch modes of Span80 on the surface of oil-in-water droplets (red) and water-in-oil droplets (blue) measured under SSP (S-sum frequency, S-visible, P-infrared) polarization combination. The vibrational modes at ~2850, ~2875, ~2902, ~2920, ~2935, and ~2965 cm⁻¹ correspond to the symmetric (s-) CH₂ stretch mode (d+), the s-CH₃ stretch mode (r+), the CH₂ Fermi resonance (d+_{FR}), the asymmetric (as-) CH₂ stretch mode (d-), the CH₃ Fermi resonance (r+_{FR}), and the as-CH₃ stretch (r-), respectively.

The amplitude ratio between the s-CH₂ mode and the s-CH₃ mode (d⁺/r⁺ ratio) is correlated to the alkyl chain conformations of the surfactant molecules at the interface. A ratio of d⁺/r⁺ \ll 1 is observed when alkyl chains are stretched in an all-trans conformation, whereas a ratio of d⁺/r⁺ > 1 corresponds to the presence of gauche defects in the surfactant monolayer.^{2,51,52} The s-CH₂ peak dominates with a d⁺/r⁺ ratio of \sim 15.2 (SI Table S3) for oil-in-water droplets, indicating that the Span80 alkyl chains form disordered structures at the surface of oil-in-water droplets.

The vibrational SFS spectrum of the inverse interface, the water-in-oil droplets, is shown as well in Figure 3C (blue data). Here, the s-CH $_2$ and s-CH $_3$ peaks have almost the same

amplitude with a d^+/r^+ ratio of ~1.1. The lower d^+/r^+ amplitude ratio at the water-in-oil droplet surface compared to the oil-in-water droplet surface indicates that Span80 molecules acquire a more ordered conformation with fewer gauche defects at the water droplets in oil interface, compared to that of the oil droplets in water. Thus, even though the interface is composed of the same chemicals, Span80 adopts a different structure, depending on whether the main phase is composed of oil or water.

The difference in the surface structure of Span80 at the two droplet interfaces is caused by the different mechanisms that impart droplet stability. Since Span80 forms a disordered monolayer at the oil-in-water droplet surface, a significant number of hydrophobic-water contact points remain on the surface. The Span80-covered hexadecane droplets have a negative ζ-potential value similar to bare hexadecane droplets in water. Span80 is a neutral surfactant and therefore does not contribute to the charge of the droplet when it is adsorbed at the interface. We therefore expect that oil droplets in water systems are stabilized via the same mechanism. Neat oil droplets in water are stable against coalescence because of electrostatic repulsion arising from their negative surface charge. This negative surface charge stems from improper Hbonds between oil C-H (charge accepting) and water O-H (charge donating) groups. 30,54,55 Charge transfer between water and oil thus ensures that neat oil droplets in water are weakly negatively charged. Water droplets in oil are not expected to be stabilized by charge transfer because charge transfer from water-to-oil requires a significant excess of water compared to oil.⁵⁵ In this system, a different stabilizing mechanism is needed that prevents the water droplets from approaching closely. Since the alkyl chains of Span80 stick out, this provides a steric barrier that prevents coalescence. The high degree of order in the alkyl chains at the droplet surface leads to this steric repulsion. There is undoubtedly also an entropic penalty for doing so, which is why it is absent for the oil droplets in water (where such additional steric hindrance is not required for stability). Both effects are not needed for extended planar interfaces, which exist because of gravity, and

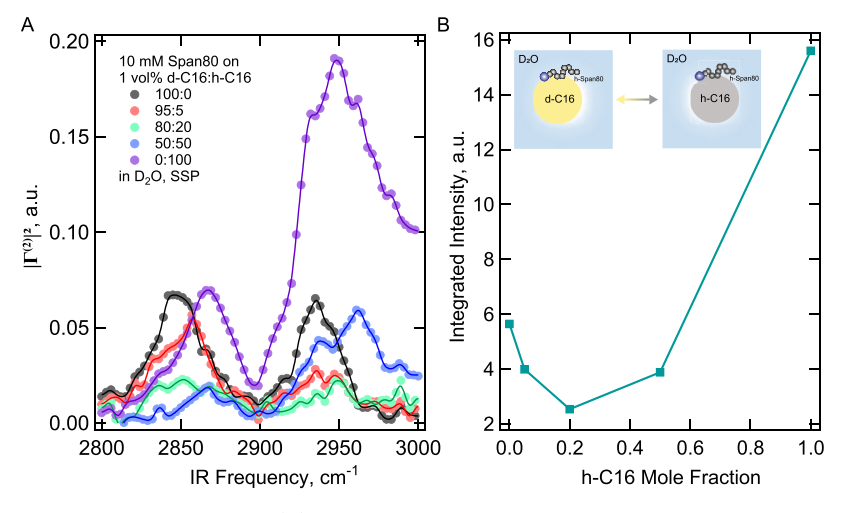


Figure 4. Interference modifies vibrational SFS spectra. (A) SFS C-H stretch spectra of 10 mM Span80 on oil-in-water droplets, where the oil phase was isotopically diluted using h-C16. Solid lines are a guide to the eye. (B) Integrated C-H intensity as a function of the mole fraction of h-C16. The inset shows a schematic illustration of both extremes.

no additional stabilizing mechanism is required to maintain the system.

Next, we investigate the effect of adding further complexity by turning on interfacial interference. To turn this on, we use oil droplets in water, with Span80, where we increase complexity by gradually replacing the C–H transparent deuterated oil d-C16 with hydrogenated oil h-C16.

Interfacial Interference. In order to investigate interference effects on the vibrational SF spectra, we modified the droplet structure in such a way that it contains chemical groups that vibrate at similar frequencies as the C-H modes of Span80. To do so, oil droplets in water were prepared with 10 mM Span80 in the aqueous solution. The oil phase was then modified by using different ratios of hydrogenated (h-C16) to deuterated (d-C16) hexadecane, using the following d-C16:h-C16 volume ratios of 100:0, 95:5, 80:20, 50:50, and 0:100. In this case, IR absorption by the oil is negligible since it only makes up 1% of the total volume. ⁴⁶ Figure 4A shows the $|\Gamma^{(2)}|^2$ spectra, which in this case are the SFS intensity spectra divided by the IR excitation profile (Figure S1). Because d-C16 and h-C16 are chemically very similar, we expect that the interfacial density and orientational distribution function of Span80 molecules remain identical at all isotopic dilution ratios.

Figure 4A shows the C-H stretch $|\Gamma^{(2)}|^2$ spectra of the oil droplet interface normalized by the incident IR profiles and droplet radii. For Span80 on d-C16 droplets (Figure 4A, black, identical to the red data in Figure 3C), the C-H stretch region consists of d^+ , r^+ , d^+_{FR} , d^- , r^+_{FR} , and r^- modes. When h-C16 replaces d-C16 in the oil phase, the electromagnetic SF fields emitted by the C-H stretch modes of the alkyl chains of Span80 and h-C16 interfere. Since the molecular structure and orientation of h-C16 and Span80 are not identical, the interference leads to a spectral distortion: Upon hydrogenation of the oil, the s-CH₂ stretch mode vanishes while other modes minimize in intensity and then increase again as a function of the amount of h-C16. The overall intensity of the C–H stretch region follows a non-monotonous trend with an initial decrease followed by an increase at high mole fractions of h-C16 (Figure 4B). An intensity minimum was observed at ~20 vol % h-C16, indicating that the destructive interference between the C-H stretch modes of Span80 and h-C16 is maximum at this concentration (Figure 4A green, Figure 4B).

The effect of interference was previously measured on the C-H stretch spectra of sodium dodecyl sulfate (SDS)-covered hexadecane droplets in water.³⁴ SDS molecules form dilute monolayers on the surface of hexadecane droplets.^{33,34} The smallest projected area at maximum surface adsorption of SDS (at the concentration of SDS around 8 mM) was found to be 4.25 nm². At this surface density, for droplets prepared with 8 mM h-SDS and 100 vol % h-C16 in the oil phase, the SF response from h-SDS molecules destructively interfered with the response from h-C16 to generate a nearly vanishing signal from the interface. Figure 4A,B show that the maximum destructive interference between dispersions containing a total amount of 10 mM Span80 occurs around 20 vol % h-C16. It is perhaps surprising that this minimum occurs at such a low intensity but can be rationalized if we assume that both molecules have broad orientational distribution functions, with comparable SF responses per C-H group.

Span80 does not form a densely packed monolayer at the oil nanodroplet surface, as is clear from the d^+/r^+ amplitude ratio of Figure 3 (\sim 15.2). In comparison to SDS, Span80 forms an even more dilute monolayer at the interface so that 20 vol % h-C16 on the droplet surface is sufficient to induce maximum destructive interference with the Span80 C-H modes. Above this concentration, the C-H stretch spectrum is dominated by the SF response from the h-C16 molecules. The overall intensity of the droplets with 100% h-C16 is three times more than that of d-C16 droplets because of the higher interfacial density of h-C16 molecules compared to Span80. The relative intensity of the d⁺ mode decreases, and the r⁺ mode increases with an increase in the concentration of h-C16. The C-H stretch spectrum of Span80 on 100% h-C16 droplets (Figure 4A, purple) resembles the spectrum of h-C16 on the surface of pure oil-in-water droplets³⁵ and those having d-SDS on their surface³⁴ (as they are identical). This further confirms that the SF response under these conditions predominantly arises from interfacial hexadecane.

Having determined that interfacial inversion and interfacial interference both lead to drastic structural changes that are both different, we use the versatility of the droplet system to investigate them when they are both relevant. To do so, we use water droplets in oil, where the oil phase is gradually hydrogenated (Figure 5A). In this case, the C–H modes in

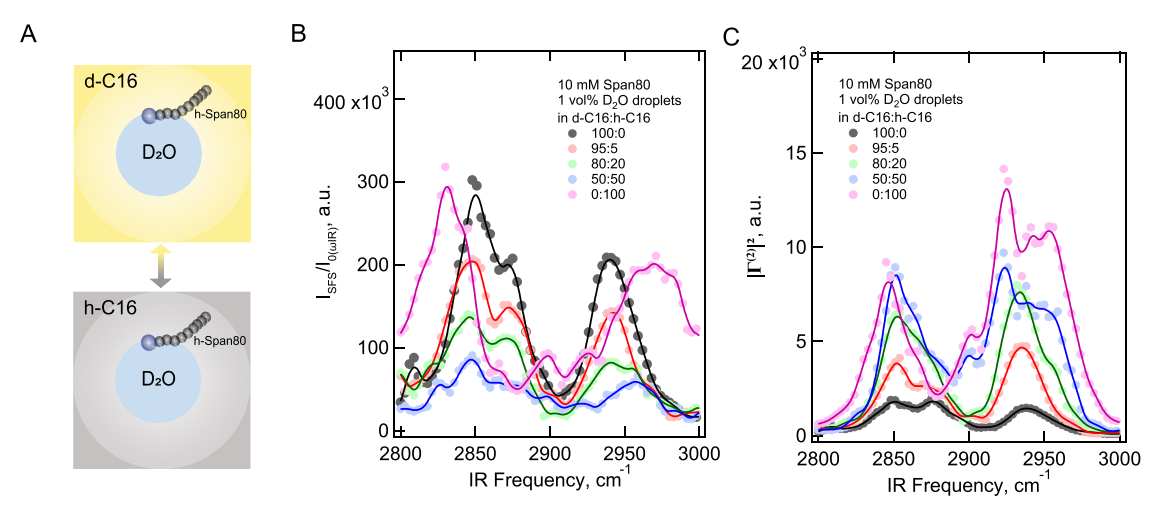


Figure 5. Effects of both interfacial interference and IR bulk phase absorption on the measured C–H spectra. (A) Schematic illustration of the isotopic dilution experiment in water-in-oil droplets. (B) C–H stretch intensity spectra of water droplets prepared with 10 mM Span80 in mixtures of different d-C16:h-C16 ratios. (C) Retrieved $|\Gamma^{(2)}|^2$ spectra of the same measurement series.

the main medium are IR absorptive in the spectral region of interest (leading to spectral modification), and they also emit interfacial SF photons in the same frequency range that interfere with the emission of the surface groups of the Span80 molecules. Under these complicated conditions, is it still possible to retrieve $|\Gamma^{(2)}|^2$?

Simultaneous Bulk IR Absorption and Interfacial Interference. To investigate the effects of IR absorption and interfacial interference on measured C-H spectra, we prepared water-in-oil droplets covered with Span80 in mixtures of d-C16:h-C16 at ratios of 100:0, 95:5, 80:20, 50:50, and 0:100. Unlike oil-in-water droplets, the C-H spectra of waterin-oil droplets are modulated by both interfacial interference and bulk IR absorption effects. Figure 5B shows the SFS intensity recorded in the C-H stretch region normalized by the incident IR intensity $(I_0(\omega_{\rm IR}))$ (raw data and incident IR profiles provided in Figure S2A). The black spectrum in Figure 5B is the C-H stretch spectrum of Span80-covered water droplets in pure d-C16. With the increase in the fraction of h-C16 in the oil phase, the IR beam gets absorbed, decreasing and spectrally modifying the overall intensity of the C-H stretch region, as was shown in Figure 2.

With 5% h-C16 added to the oil phase, the overall intensity of the C-H stretch region dropped by ~20%. With a further increase in the fraction of h-C16 in the oil phase, the SF intensity continues to decrease until 50% h-C16. At 100% h-C16, the intensity of the C-H stretch region was higher again, with apparent peak frequencies shifting drastically compared to 100% d-C16. These changes in intensity with an increase in the fraction of h-C16 results from a combination of absorption and interference effects. Correcting for the IR absorption using the transmission spectra in Figure S2B, we obtain the $|\Gamma^{(2)}|^2$ spectra of Figure 5C. These spectra now report on the combined second-order polarization emitted by all interfacial C-H modes (Span80 and h-C16). They are different from the ones in Figure 4A because (1) interfacial structures of inverted interfaces are different as they result from stabilizing droplets in systems that have different inter-droplet interactions (as we saw in Figures 3A,B) and (2) the interfering oil phase is the outside/main medium, which generally leads to different interferences from a situation where the interfering compounds are on the inside.56

Thus, it is possible to derive $|\Gamma^{(2)}|^2$ spectra, even for very complex combinations of substances and optical effects, and this confirms vibrational SF spectroscopy into a very potent method to understand molecular structure on the nanoscale and to use it to investigate the interplay between local interfacial structure and longer-range particle—particle interactions, even when absorption and interference play obstructing roles. These advances will aid the investigation of more complex soft matter or nanoparticle systems.

CONCLUSIONS

We measured and analyzed, using considerations on spectrally complex bulk phase absorption, vibrational SFS spectra of several different nanodroplets systems all composed of the same chemicals (hexadecane, water, and Span80), investigating the influence of interfacial inversion (reversing the main and droplet phases), interfacial interference (by including identical chemical groups in one of the bulk phases), and a combination of IR absorption and interference (by having identical chemical groups in the main phase and at the interface, with sharp resonant features). For all cases, we find that appropriate analysis allows the extraction of the effective surface susceptibility $(|\Gamma^{(2)}|^2)$ spectrum, which represents the vibrational sum frequency response from the interface.

Exchanging the droplet phase (from d-C16 to D_2O) and the main phase (from D_2O to d-C16) results in an inverted interface, which has different $|\Gamma^{(2)}|^2$ spectra. These spectra reflect different structures that find their origin in the different interactions needed to stabilize the nanodrops: oil droplets have interfacial Span80 molecules that are very disordered with many conformational defects. This disordered conformation of Span80 enables water-to-oil charge transfer interactions, and the resulting negative charge stabilizes the droplets against coalescence via electrostatic repulsion. Water droplets, on the other hand, have Span80 molecules with their alkyl chains extending further into the main phase. The steric hindrance provided by these more ordered alkyl chains stabilizes the water droplets in oil.

Replacing the oil in both systems with hydrogenated oil adds further complexity to the interactions: for oil droplets, this adds interfacial interference, and for water droplets, this adds interfacial interference as well as absorption of the IR beam. In the first case, the spectra change drastically, and based on the location of maximum interference, one can estimate the surface density ratio of participating molecules. In the second case, the same process happens, but this can only be determined once the absorption effects have been accounted for using the $|\Gamma^{(2)}|^2$ spectrum and not the intensity spectrum.

This investigation further advances the understanding and the possibilities and uses of vibrational SFS to link structure and function on different length scales and with advancing chemical complexity.

ASSOCIATED CONTENT

50 Supporting Information

The Supporting Information is available free of charge at https://pubs.acs.org/doi/10.1021/acs.jpcb.3c02727.

Table with parameters used to simulate input $|\Gamma^{(2)}|^2$ in Figure 2 (Table S1); table with size distribution of the prepared droplets (Table S2); table of fit parameters used to fit the spectra in Figure 3 (Table S3); and figures containing raw data before analysis (PDF)

AUTHOR INFORMATION

Corresponding Author

S. Roke — Laboratory for Fundamental BioPhotonics, Institute of Bioengineering (IBI), School of Engineering (STI), École Polytechnique Fédérale de Lausanne (EPFL), CH-1015 Lausanne, Switzerland; Institute of Materials Science and Engineering (IMX), School of Engineering (STI) and Lausanne Centre for Ultrafast Science, École Polytechnique Fédérale de Lausanne (EPFL), CH-1015 Lausanne, Switzerland; orcid.org/0000-0002-6062-7871; Email: sylvie.roke@epfl.ch

Authors

- S. Pullanchery Laboratory for Fundamental BioPhotonics, Institute of Bioengineering (IBI), School of Engineering (STI), École Polytechnique Fédérale de Lausanne (EPFL), CH-1015 Lausanne, Switzerland; orcid.org/0000-0002-7011-0788
- L. Zhang Laboratory for Fundamental BioPhotonics, Institute of Bioengineering (IBI), School of Engineering (STI), École Polytechnique Fédérale de Lausanne (EPFL), CH-1015 Lausanne, Switzerland
- S. Kulik Laboratory for Fundamental BioPhotonics, Institute of Bioengineering (IBI), School of Engineering (STI), École Polytechnique Fédérale de Lausanne (EPFL), CH-1015 Lausanne, Switzerland

Complete contact information is available at: https://pubs.acs.org/10.1021/acs.jpcb.3c02727

Author Contributions

S.P. and L.Z. contributed equally.

Notes

The authors declare no competing financial interest.

ACKNOWLEDGMENTS

This work is supported by the Swiss National Science Foundation grant 200021-182606-1 (S.P. and S.K.) and European Research Council grant agreement no. 951324 H2020, R2-tension (L.Z.). S.R. thanks the Julia Jacobi Foundation. Authors thank Dr. Benjamin Rehl for useful discussions.

REFERENCES

- (1) Du, Q.; Superfine, R.; Freysz, E.; Shen, Y. R. Vibrational Spectroscopy of Water at the Vapor/Water Interface. *Phys. Rev. Lett.* **1993**, 70, 2313–2316.
- (2) Guyot-Sionnest, P.; Hunt, J. H.; Shen, Y. R. Sum-Frequency Vibrational Spectroscopy of a Langmuir Film: Study of Molecular Orientation of a Two-Dimensional System. *Phys. Rev. Lett.* **1987**, *59*, 1597–1600.
- (3) Harris, A. L.; Chidsey, C. E. D.; Levinos, N. J.; Loiacono, D. N. Monolayer Vibrational Spectroscopy by Infrared-Visible Sum Generation at Metal and Semiconductor Surfaces. *Chem. Phys. Lett.* **1987**, *141*, 350–356.
- (4) Hunt, J. H.; Guyot-Sionnest, P.; Shen, Y. R. Observation of C-H Stretch Vibrations of Monolayers of Molecules Optical Sum-Frequency Generation. *Chem. Phys. Lett.* **1987**, *133*, 189–192.
- (5) Shultz, M. J.; Schnitzer, C.; Simonelli, D.; Baldelli, S. Sum Frequency Generation Spectroscopy of the Aqueous Interface: Ionic and Soluble Molecular Solutions. *Int. Rev. Phys. Chem.* **2000**, *19*, 123–153.
- (6) Liu, J.; Conboy, J. C. Phase Transition of a Single Lipid Bilayer Measured by Sum-Frequency Vibrational Spectroscopy. *J. Am. Chem. Soc.* **2004**, *126*, 8894–8895.
- (7) Scatena, L. F.; Brown, M. G.; Richmond, G. L. Water at Hydrophobic Surfaces: Weak Hydrogen Bonding and Strong Orientation Effects. *Science* **2001**, 292, 908.
- (8) Stiopkin, I. V.; Weeraman, C.; Pieniazek, P. A.; Shalhout, F. Y.; Skinner, J. L.; Benderskii, A. V. Hydrogen Bonding at the Water Surface Revealed by Isotopic Dilution Spectroscopy. *Nature* **2011**, 474, 192–195.
- (9) Strazdaite, S.; Versluis, J.; Backus, E. H. G.; Bakker, H. J. Enhanced Ordering of Water at Hydrophobic Surfaces. *J. Chem. Phys.* **2014**, *140*, No. 054711.
- (10) Hosseinpour, S.; Roeters, S. J.; Bonn, M.; Peukert, W.; Woutersen, S.; Weidner, T. Structure and Dynamics of Interfacial Peptides and Proteins from Vibrational Sum-Frequency Generation Spectroscopy. *Chem. Rev.* **2020**, *120*, 3420–3465.
- (11) Richmond, G. L. Structure and Bonding of Molecules at Aqueous Surfaces. *Annu. Rev. Phys. Chem.* **2001**, *52*, 357–389.
- (12) Eisenthal, K. B. Liquid Interfaces Probed by Second-Harmonic and Sum-Frequency Spectroscopy. *Chem. Rev.* **1996**, *96*, 1343–1360.
- (13) Yan, E. C. Y.; Fu, L.; Wang, Z.; Liu, W. Biological Macromolecules at Interfaces Probed by Chiral Vibrational Sum Frequency Generation Spectroscopy. *Chem. Rev.* **2014**, *114*, 8471–8498.
- (14) Geiger, F. M. Second Harmonic Generation, Sum Frequency Generation, and X(3): Dissecting Environmental Interfaces with a Nonlinear Optical Swiss Army Knife. *Annu. Rev. Phys. Chem.* **2009**, *60*, 61–83
- (15) Gibbs-Davis, J. M.; Kruk, J. J.; Konek, C. T.; Scheidt, K. A.; Geiger, F. M. Jammed Acid-Base Reactions at Interfaces. *J. Am. Chem. Soc.* **2008**, *130*, 15444–15447.
- (16) Jubb, A. M.; Hua, W.; Allen, H. C. Environmental Chemistry at Vapor/Water Interfaces: Insights from Vibrational Sum Frequency Generation Spectroscopy. *Annu. Rev. Phys. Chem.* **2012**, *63*, 107–130.
- (17) Nihonyanagi, S.; Mondal, J. A.; Yamaguchi, S.; Tahara, T. Structure and Dynamics of Interfacial Water Studied by Heterodyne-Detected Vibrational Sum-Frequency Generation. *Annu. Rev. Phys. Chem.* **2013**, *64*, 579–603.
- (18) Lu, R.; Gan, W.; Wu, B.-h.; Zhang, Z.; Guo, Y.; Wang, H.-f. C—H Stretching Vibrations of Methyl, Methylene and Methine Groups at the Vapor/Alcohol (N = 1–8) Interfaces. *J. Phys. Chem. B* **2005**, *109*, 14118–14129.
- (19) Ma, G.; Allen, H. C. Dppc Langmuir Monolayer at the Air—Water Interface: Probing the Tail and Head Groups by Vibrational Sum Frequency Generation Spectroscopy. *Langmuir* **2006**, *22*, 5341—5349.
- (20) Wang, H.-F.; Velarde, L.; Gan, W.; Fu, L. Quantitative Sum-Frequency Generation Vibrational Spectroscopy of Molecular

- Surfaces and Interfaces: Lineshape, Polarization, and Orientation. Annu. Rev. Phys. Chem. 2015, 66, 189-216.
- (21) Hore, D. K.; Beaman, D. K.; Richmond, G. L. Surfactant Headgroup Orientation at the Air/Water Interface. *J. Am. Chem. Soc.* **2005**, 127, 9356–9357.
- (22) Roke, S.; Roeterdink, W. G.; Wijnhoven, J. E. G. J.; Petukhov, A. V.; Kleyn, A. W.; Bonn, M. Vibrational Sum Frequency Scattering from a Submicron Suspension. *Phys. Rev. Lett.* **2003**, *91*, No. 258302.
- (23) Roke, S.; Gonella, G. Nonlinear Light Scattering and Spectroscopy of Particles and Droplets in Liquids. *Annu. Rev. Phys. Chem.* **2012**, *63*, 353–378.
- (24) Roke, S.; Bonn, M.; Petukhov, A. V. Nonlinear Optical Scattering: The Concept of Effective Susceptibility. *Phys. Rev. B* **2004**, 70, No. 115106.
- (25) Roke, S.; Buitenhuis, J.; van Miltenburg, J. C.; Bonn, M.; van Blaaderen, A. Interface—Solvent Effects During Colloidal Phase Transitions. *J. Phys.: Condens. Matter* **2005**, *17*, S3469.
- (26) Roke, S.; Berg, O.; Buitenhuis, J.; van Blaaderen, A.; Bonn, M. Surface Molecular View of Colloidal Gelation. *Proc. Natl. Acad. Sci. U.S.A.* **2006**, *103*, 13310–13314.
- (27) de Beer, A. G. F.; de Aguiar, H. B.; Nijsen, J. F. W.; Roke, S. Detection of Buried Microstructures by Nonlinear Light Scattering Spectroscopy. *Phys. Rev. Lett.* **2009**, *102*, No. 095502.
- (28) de Aguiar, H. B.; de Beer, A. G. F.; Roke, S. The Presence of Ultralow Densities of Nanocrystallites in Amorphous Poly(Lactic Acid) Microspheres. *J. Phys. Chem. B* **2013**, *117*, 8906–8910.
- (29) Samson, J.-S.; Scheu, R.; Smolentsev, N.; Rick, S. W.; Roke, S. Sum Frequency Spectroscopy of the Hydrophobic Nanodroplet/Water Interface: Absence of Hydroxyl Ion and Dangling Oh Bond Signatures. *Chem. Phys. Lett.* **2014**, *615*, 124–131.
- (30) Pullanchery, S.; Kulik, S.; Rehl, B.; Hassanali, A.; Roke, S. Charge Transfer across C-H···O Hydrogen Bonds Stabilizes Oil Droplets in Water. *Science* **2021**, 374, 1366–1370.
- (31) Pullanchery, S.; Kulik, S.; Roke, S. Water Structure at the Hydrophobic Nanodroplet Surface Revealed by Vibrational Sum Frequency Scattering Using Isotopic Dilution. *J. Phys. Chem. B* **2022**, 126, 3186–3192.
- (32) Vácha, R.; Rick, S. W.; Jungwirth, P.; de Beer, A. G. F.; de Aguiar, H. B.; Samson, J.-S.; Roke, S. The Orientation and Charge of Water at the Hydrophobic Oil Droplet—Water Interface. *J. Am. Chem. Soc.* **2011**, *1*33, 10204—10210.
- (33) de Aguiar, H. B.; de Beer, A. G. F.; Strader, M. L.; Roke, S. The Interfacial Tension of Nanoscopic Oil Droplets in Water Is Hardly Affected by Sds Surfactant. J. Am. Chem. Soc. 2010, 132, 2122–2123.
- (34) de Aguiar, H. B.; Strader, M. L.; de Beer, A. G. F.; Roke, S. Surface Structure of Sodium Dodecyl Sulfate Surfactant and Oil at the Oil-in-Water Droplet Liquid/Liquid Interface: A Manifestation of a Nonequilibrium Surface State. *J. Phys. Chem. B* **2011**, *115*, 2970–2978
- (35) Scheu, R.; Chen, Y.; de Aguiar, H. B.; Rankin, B. M.; Ben-Amotz, D.; Roke, S. Specific Ion Effects in Amphiphile Hydration and Interface Stabilization. *J. Am. Chem. Soc.* **2014**, *136*, 2040–2047.
- (36) Zdrali, E.; Chen, Y.; Okur, H. I.; Wilkins, D. M.; Roke, S. The Molecular Mechanism of Nanodroplet Stability. *ACS Nano* **2017**, *11*, 12111–12120.
- (37) Zdrali, E.; Okur, H. I.; Roke, S. Specific Ion Effects at the Interface of Nanometer-Sized Droplets in Water: Structure and Stability. *J. Phys. Chem. C* **2019**, *123*, 16621–16630.
- (38) Hensel, J. K.; Carpenter, A. P.; Ciszewski, R. K.; Schabes, B. K.; Kittredge, C. T.; Moore, F. G.; Richmond, G. L. Molecular Characterization of Water and Surfactant Aot at Nanoemulsion Surfaces. *Proc. Natl. Acad. Sci. U.S.A.* **2017**, *114*, 13351–13356.
- (39) Chen, Y.; Jena, K. C.; Lütgebaucks, C.; Okur, H. I.; Roke, S. Three Dimensional Nano "Langmuir Trough" for Lipid Studies. *Nano Lett.* **2015**, *15*, 5558–5563.
- (40) Chen, Y.; Okur, H. I.; Lütgebaucks, C.; Roke, S. Zwitterionic and Charged Lipids Form Remarkably Different Structures on Nanoscale Oil Droplets in Aqueous Solution. *Langmuir* **2018**, *34*, 1042–1050.

- (41) Okur, H. I.; Chen, Y.; Smolentsev, N.; Zdrali, E.; Roke, S. Interfacial Structure and Hydration of 3d Lipid Monolayers in Aqueous Solution. *J. Phys. Chem. B* **2017**, *121*, 2808–2813.
- (42) Smolentsev, N.; Lütgebaucks, C.; Okur, H. I.; de Beer, A. G. F.; Roke, S. Intermolecular Headgroup Interaction and Hydration as Driving Forces for Lipid Transmembrane Asymmetry. *J. Am. Chem. Soc.* **2016**, *138*, 4053–4060.
- (43) Johansson, P. K.; Koelsch, P. Vibrational Sum-Frequency Scattering for Detailed Studies of Collagen Fibers in Aqueous Environments. J. Am. Chem. Soc. 2014, 136, 13598–13601.
- (44) Golbek, T. W.; Strunge, K.; Chatterley, A. S.; Weidner, T. Peptide Orientation at Emulsion Nanointerfaces Dramatically Different from Flat Surfaces. *J. Phys. Chem. Lett.* **2022**, *13*, 10858–10862.
- (45) Olenick, L. L.; Troiano, J. M.; Smolentsev, N.; Ohno, P. E.; Roke, S.; Geiger, F. M. Polycation Interactions with Zwitterionic Phospholipid Monolayers on Oil Nanodroplet Suspensions in Water (D20) Probed by Sum Frequency Scattering. *J. Phys. Chem. B* **2018**, 122, 5049–5056.
- (46) Kulik, S.; Pullanchery, S.; Roke, S. Vibrational Sum Frequency Scattering in Absorptive Media: A Theoretical Case Study of Nano-Objects in Water. *J. Phys. Chem. C* **2020**, *124*, 23078–23085.
- (47) de Aguiar, H. B.; Samson, J.-S.; Roke, S. Probing Nanoscopic Droplet Interfaces in Aqueous Solution with Vibrational Sum-Frequency Scattering: A Study of the Effects of Path Length, Droplet Density and Pulse Energy. *Chem. Phys. Lett.* **2011**, *512*, 76–80.
- (48) de Aguiar, H. B.; Scheu, R.; Jena, K. C.; de Beer, A. G. F.; Roke, S. Comparison of Scattering and Reflection Sfg: A Question of Phase-Matching. *Phys. Chem. Chem. Phys.* **2012**, *14*, 6826–6832.
- (49) Sugiharto, A. B.; Johnson, C. M.; de Aguiar, H. B.; Alloatti, L.; Roke, S. Generation and Application of High Power Femtosecond Pulses in the Vibrational Fingerprint Region. *Appl. Phys. B* **2008**, *91*, 315–318.
- (50) Smolentsev, N.; Smit, W. J.; Bakker, H. J.; Roke, S. The Interfacial Structure of Water Droplets in a Hydrophobic Liquid. *Nat. Commun.* **2017**, *8*, No. 15548.
- (51) Esenturk, O.; Walker, R. A. Surface Vibrational Structure at Alkane Liquid/Vapor Interfaces. *J. Chem. Phys.* **2006**, *125*, No. 174701.
- (52) Tyrode, E.; Hedberg, J. A Comparative Study of the Cd and Ch Stretching Spectral Regions of Typical Surfactants Systems Using Vsfs: Orientation Analysis of the Terminal Ch3 and Cd3 Groups. *J. Phys. Chem. C* **2012**, *116*, 1080–1091.
- (53) Note that the d+/r+ amplitude ratio of water-in-oil droplets appears to be different from the spectrum that was reported in Ref 50. This difference is caused by the difference in spectral analysis and the use of $|\Gamma \wedge ((2))| \wedge 2$ instead of the raw data.
- (54) Pullanchery, S.; Kulik, S.; Okur, H. I.; de Aguiar, H. B.; Roke, S. On the Stability and Necessary Electrophoretic Mobility of Bare Oil Nanodroplets in Water. *J. Chem. Phys.* **2020**, *152*, No. 241104.
- (55) Poli, E.; Jong, K. H.; Hassanali, A. Charge Transfer as a Ubiquitous Mechanism in Determining the Negative Charge at Hydrophobic Interfaces. *Nat. Commun.* **2020**, *11*, No. 901.
- (56) Smolentsev, N.; Roke, S. Self-Assembly at Water Nanodroplet Interfaces Quantified with Nonlinear Light Scattering. *Langmuir* **2020**, *36*, 9317–9322.